Compression of Plasma to Megabar Range using Imploding Liner

J. H. Degnan, M. L. Alme,* B. S. Austin, J. D. Beason, S. K. Coffey,† D. G. Gale,‡ J. D. Graham,‡ J. J. Havranek, T. W. Hussey, G. F. Kiuttu, B. B. Kreh, F. M. Lehr, R. A. Lewis,§ D. E. Lileikis, D. Morgan,‖ C. A. Outten,¶ R. E. Peterkin, Jr., D. Platts,‖ N. F. Roderick,** E. L. Ruden, U. Shumlak,†† G. A. Smith,§ W. Sommars,‡ and P. J. Turchi‡‡

Air Force Research Laboratory, Directed Energy Directorate, Kirtland AFB, New Mexico 87117-5776

(Received 19 August 1998)

Axial current discharges were used to implode spherical aluminum shells with thickness tapered to match the external magnetic pressure. These implosions were used to compress hydrogen plasmas with an initial pressure >100 bar and an initial temperature >1 eV. The implosion and compressed plasma effect on a central target were observed radiographically. The target's radius vs time indicates that the plasma pressure reaches ~1 Mbar prior to liner-target contact. [S0031-9007(99)08774-8]

PACS numbers: 52.55.Ez, 52.50.Lp

We report on experiments to produce and compress plasmas to Mbar pressure. Fluid with an isotropic pressure in the Mbar range may be useful for compressing targets in fusion experiments, for equation of state experiments, for accelerating small projectiles to hypersonic velocities, and for other high energy density experiments. While these experiments were not for fusion applications, they are relevant to magnetized target fusion (MTF), such as described by Lindemuth *et al.* [1,2], and by Chernyshev *et al.* [3]. A variant of these experiments, using magnetized, lower density deuterium instead of unmagnetized, higher density hydrogen, would be an MTF experiment. A number of researchers have suggested the concept of using imploding liners to compress plasmas (e.g., [4–8]).

We used a capacitor bank (Shiva Star) operated at 12 MA and 5 MJ to implode aluminum shells (aka liners) electromagnetically in tapered, quasispherical geometry, achieving peak implosion velocities above 20 km/s inner surface (~10 km/s thickness averaged) [9]. The discharge current has a sinusoidal waveform with ~9 μs rise time. Lower velocity (up to 2 km/s), quasispherical solid liner implosions have also been reported by Goloviznin [10], Chernyshev [11], and Mokhov [12]. Cylindrical implosions of Al shells that were suitable for compressing plasmas (but without inserted plasmas) were reported by Sherwood [13]. Lower velocity implosions of cylindrical metal liners, intended for use in compressing magnetized plasmas, were reported by Turchi [14].

We have used the present implosions to compress a hydrogen plasma with initial pressure above 100 bars and initial temperature above 1 eV. We use H that is initially hot enough to insure that the sound speed in this fluid will be greater than the velocity of the inner surface of the imploding solid liner; this avoids shock formation in the compressed plasma. In these experiments, we prevent magnetization of the plasma, in an attempt to obtain uniform, isotropic fluid pressure. We have obtained experimental (radiographic) evidence of compressing the plasma to pressures ~Mbar, prior to contact of the outer liner with the interior shell.

The initial H plasma is obtained using a 1 MA, 350 kJ coaxial plasma gun and is injected into the interior of a metal shell liner, through a circular array of metal vanes to strip away an azimuthal magnetic field [15,16]. A discharge of the Shiva Star capacitor bank then implodes the liner.

Plasma injection was observed with auxiliary experiments, using chambers similar to the initial interior volume of the solid liner, but with greater diagnostic access. Diagnostics included time-gated optical spectroscopy, fast photography, and piezoelectric probes. Inductive magnetic probes are used to monitor current delivery to the vicinity of the injection vanes and to confirm the absence of a magnetic field in the chamber. Piezoelectric probe signals indicate that plasma with pressures up to 100 bars is injected into the interior of cylindrical solid liners [17]. This is consistent with 2D-MHD simulations [16,18]. Such simulations indicate that plasma at pressures of 170 bars is injected into the interior of our quasispherical liners. Optical spectroscopy suggests that the plasma temperature is somewhat higher than 1 eV.

The imploding Al shell is observed with radiography. The effect of the compressed plasma on a cylindrical shell of Cu, serving as a compression target, is also observed with radiography. The Al spherical shell is initially 8 cm in diameter, with a thickness that tapers from 1 to 2 mm, from the midplane of the electrode gap to the contacts of the liner at each electrode. The liner is mounted between two conical electrodes of steel. See Fig. 1. The interelectrode gap converges at an included angle of 90° to a minimum value of 1 cm. The Al shell thickness is proportional to the cosecant squared of the polar angle and is thinnest at a 90° angle from the central axis. To first order, this taper causes the ratio of magnetic pressure to liner mass per unit area (and the spherically radial acceleration) to remain independent of the polar angle. The result is a nominally spherical implosion. Radiographs are taken through the 0.6 cm thick aluminum outer (return current) conductor. The target is a 1 cm tall, 0.34 cm radius, Cu tube with tapered thickness (0.15 to 0.38 mm). The operating

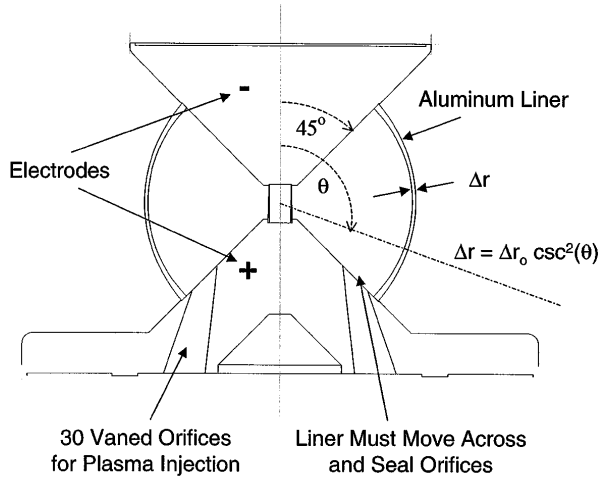

FIG. 1. Liner, electrode, and plasma injection geometry.

parameters of the radiography source are 300 kV, 5 kA, 30 ns pulse, with a tungsten anode. The spatial resolution is ~0.2 mm. Radiographs, shown in Fig. 2, show compression of the target cylinder prior to contact of its outer surface with the inner surface of the imploding liner. We can see the reduced exposure indicating the compressed plasma layer between the imploding liner inner surface and the central target outer surface until less than 0.1 μs before contact of the two surfaces. A series of such radiographs has enabled estimates of the average acceleration of the inner target surface and the plasma pressure during two time intervals late in the implosion—compression. These indicate that the plasma pressure reaches ~Mbar prior to contact (see Fig. 3 and Table I).

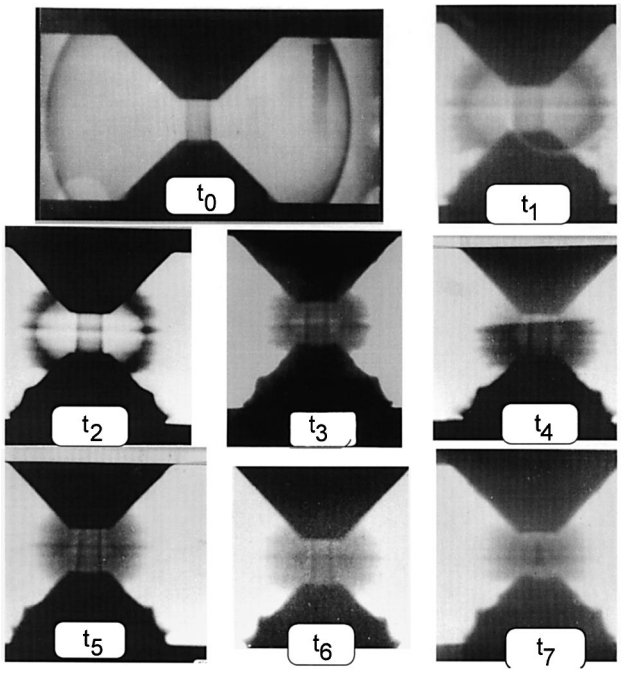

FIG. 2. Implosion-plasma compression radiographs show central target compression. The times after the start of current discharge are t_0 through t_7: 0.0, 13.48, 13.59, 14.38, 14.44, 14.52, 14.61, and 14.73 μs, respectively. One can see the reduced exposure indicating the compressed plasma layer between the imploding liner inner surface and the central target outer surface until less than 0.1 μs before contact of the two surfaces.

The radiographs show some instability growth—somewhat more than in similar implosions with no interior plasma. These implosions were operated at aggressive parameters, close to the limiting criteria for material strength stabilization [19] and avoiding early bulk melting.

The estimates of plasma pressure are done by obtaining the radius of the outer surface of the target shell at the midelectrode gap, for three successive radiographs ($r_{n'}$, $r_{n+1'}$, and r_{n+2} at $t_{n'}$, $t_{n+1'}$, and t_{n+2}). From these three radii, we obtain the average velocity over two successive time intervals, $v_{n,n+1} = (r_{n+1} - r_n)/(t_{n+1} - t_n)$ and $v_{n+1,n+2} = (r_{n+2} - r_{n+1})/(t_{n+2} - t_{n+1})$ at times $\tau_{n,n+1} = 0.5(t_n + t_{n+1})$ and $\tau_{n+1,n+2} = 0.5(t_{n+1} + t_{n+2})$, and the average acceleration $a_{n,n+1,n+2} = (v_{n+1,n+2} - v_{n,n+1})/(\tau_{n+1,n+2} - \tau_{n,n+1})$ over the time interval of the three successive radiographs $\tau^a_{n,n+1,n+2}$. We then equate the mass per unit area of the target shell σ times the average acceleration a to the average plasma pressure P. This is true if the target shell thickness $\delta r \ll r$, and this underestimates the average pressure P if δr is not $\ll r$. Initially, $\delta r = 2.67 \times 10^{-2}$ cm at the midgap, and $r = 3.3 \times 10^{-1}$ cm. Thus, the initial mass per unit area σ_0 of the Cu shell at midgap is 0.24 g/cm^2 = 2.4 kg/m^2. Cylindrical convergence causes this to increase as r decreases: $\sigma = \sigma_0 (r_0/r)$ (if material density is not compressed). The peak plasma pressure during this interval should exceed the average.

The error bars in Fig. 3, which are a generous estimate of the radiograph resolution, exceed the spread of positional analysis results for multiple human analysts and analyses. Several analyses indicated average pressures from 0.24 to 0.95 Mbar in the first time interval, and ~3 Mbar in the second. The error bars indicate a larger uncertainty in the estimated pressure at $\tau^a_{4,5,6} = 14.52$ μs, and a ± factor of 2 uncertainty at $\tau^a_{5,6,7} = 14.62$ μs.

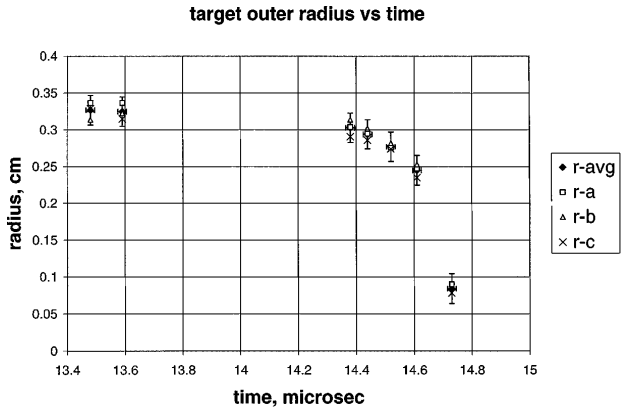

FIG. 3. Central target compression data (at midelectrode gap) indicate time average plasma pressures (over three data points) approaching a Mbar ~0.1 μs prior to contact of the liner and target. These seven data points were from three virtually identical shots; three were from the same shot.

TABLE I. Summary of the analysis of compressed fluid pressure.

Shot	n	t_n (μsec)	r_n (cm)	$v_{n,n+1}$ (cm/μs)	$\tau_{n,n+1}$ (μsec)	$a_{n,n+1,n+2}$ (cm μsec^{-2})	$\tau^a_{n,n+1,n+2}$ (μsec)	$P = \sigma a, Pa$ $\sigma = \sigma_0(r_0/r)$
	0	0.0	0.329					
1	1	13.48	0.327					
1	2	13.59	0.325					
2	3	14.38	0.303					
3	4	14.44	0.294	0.213	14.48	1.682	14.52	4.6×10^{10}
3	5	14.52	0.277	0.356	14.565	9.37	14.62	3.0×10^{11}
3	6	14.61	0.245	1.34	14.67			
2	7	14.73	0.084					

Possible sources of systematic error include a 2% tolerance in the electrode gap in the target region (which would have the same relative effect on all data points), optical depth effects which may cause the perceived outer surface of the target to be within the target shell material, and blurring due to velocity times the radiograph exposure duration (30 ns). Indeed, there is a slight difference between the specified target radius (0.34 cm), and that perceived by static radiographs (0.33 cm). This difference is about half the initial shell thickness, and we believe this is due to optical depth effects. In the incompressible approximation, this should result in the perceived outer surface being a fixed fraction of shell thickness within the outer surface. Velocity blurring may cause a radial spread of the image of approximately 0.01 cm for r_6, and approximately 0.03 cm for r_7. Such blurring may cause the perceived outer surface to be at a larger radius than at the center of the radiography exposure time, causing an underestimate of the velocity, acceleration, and external pressure.

The compressed plasma pressure estimated from the compression of the target shell is in the range expected for the observed ratio of initial to compressed volume ratio, initial plasma pressure (170 bars), and a plasma specific heat ratio of approximately 1.4. That is,

$$P = P_0(V_0/V)^\gamma, \qquad \gamma = 1.4\,.$$

This specific heat ratio accounts for the ionization energy and radiation losses in the plasma [20]. 2D-MHD simulations, using the code MACH2 [18], give similar results, without assumptions on the specific heat ratio, but treating ionization, radiation, and thermal conduction losses. The initial plasma volume is approximately 176 cm^3. Just after closure of the orifice by the liner implosion, the remaining fluid volume is approximately 54 cm^3. 2D-MHD simulations (using MACH2) indicate that the fluid pressure increases during this closure, despite some limited outflow through the injection orifices. The calculated fluid pressure inside the volume enclosed by the electrodes and the liner is approximately 1000 bars when the inner surface of the liner has passed the inner boundary of the injection orifices. Perhaps the limitation on outflow is due to fluid inertia, fluid pressure, and magnetic pressure upstream of the injection orifices. At any rate, this paper is primarily empirical, and these (and similar) simulations will be discussed more completely in a future paper. Even if there were no increase in fluid pressure until this boundary were crossed, subsequent compression of the remaining trapped fluid to a layer $\sim$ a mm thick around the target would approach a Mbar pressure. This would be 0.5 Mbar for a 0.25 cm radius, 1-mm-thick fluid layer, with 170 bar pressure at the closure of the injection orifices.

Radiation losses are expected to be small, because the hydrogen is optically thick initially, and more so during compression [20–22]. If one considers the bremsstrahlung and recombination power densities, $P_b = (1.69 \times 10^{-32}) n_e^2 T_e^{0.5}$ W/cm^3, and $P_{\rm rc} = (4.6 \times 10^{-31}) n_e^2 T_e^{-0.5}$ W/cm^3 (where $n_{e'} T_e$ = electron density in cm^{-3}, electron temperature in eV, and no heavy impurities assumed), and compares them to the black body power per unit area, one requires very small radius fluid elements for them to be comparable. That is, the optical depth for the initial fluid ($\sim 10^{20}$ cm^{-3}, $\sim$1 eV), is $\sim$0.01 cm, and it shrinks more rapidly than the fluid volume radius. This depth is $\sim$ nanometers when the fluid volume is compressed to a few tenths of cm^3. Although radiation losses are small, the radiation effects include vaporization of boundary surfaces very soon after the fluid temperature reaches $\sim$5 eV [20,22]. One can estimate this fluid temperature using $T = T_0(V_0/V)^{\gamma-1}$, where $T_0 \sim 1$ eV. This suggests that T reaches $\sim$5 eV $\sim$ 1 μs prior to liner-target contact, and $\sim$10 to 20 eV in the $\sim$0.1 μs prior to liner-target contact. The radiation heating of the Cu target is expected to produce a vapor exhaust pressure that remains small compared to fluid pressure. For example, when the fluid volume is compressed to a 2 mm layer around the Cu target, whose radius is now $\sim$0.28 cm, the fluid volume is $\sim$0.4 cm^3, the fluid pressure, temperature will be $\sim$0.8 Mbar, $\sim$11 eV, assuming $\gamma = 1.4$ behavior applies. This corresponds to a radiation power density of $\sim 1.5 \times 10^9$ W/cm^2, which vaporizes 2.4×10^5 g/cm^2 sec of Cu, resulting in an exhaust pressure of 20 kbar (assuming an exhaust velocity of 800 m/sec, due to a vaporization temperature of 0.25 eV). This estimated exhaust pressure is much less than the fluid pressure. Such estimates indicate that the total number of Cu atoms evaporated from the Cu target is $\sim$1% of the number of fluid (H) atoms. The vast majority of these are evaporated in the last $\sim$0.1 μs before liner-target contact.

These estimates are conservative in that they ignore the temperature gradient and opacity effects that reduce the radiant flux incident on the Cu target (and electrode and liner) surface. Possible initial impurities caused by the injection of the plasma through the orifice-vane structure would have to be $\sim 10^3$ of the plasma particle number to double the plasma radiation, which would have a small effect on the above estimates. While time-gated optical spectroscopy showed no evidence of such impurities [15–17], vacuum ultraviolet spectroscopy would be more likely to succeed in observing such impurities [20–22]. Such initial impurities will substantially limit the heating and pressure increase of the compressed plasma if they exceed a few tenths of a percent.

The fluid volume at the center of the first time interval for the average acceleration measurement (14.52 μs) is ~ 0.4 cm^3. This volume is an ~ 2 mm layer around the Cu target. Several analyses of the radiographic data indicate average fluid pressure of 0.24 to 0.95 Mbar in this time interval. This corresponds to a fluid pressure volume product $PV \sim 9.6$ to 38 kJ. The initial fluid PV was ~ 3 kJ. The ratio of PV^γ (for $\gamma = 1.4$) at 14.52 μs vs initial is ~ 0.25 to 1, for these pressure estimates. The estimated radiation energy loss rate at this time, using the estimated fluid temperature (~ 11 eV), assuming black body radiation, and using the Cu target surface area, is $\sim 3 \times 10^9$ W. We can expect radiation losses of several hundred J in the late stages of fluid compression. At this time, the liner kinetic energy is ~ 1 MJ [9].

Experiments with such a target and no injected plasma, but with injection ports, and with magnetic probes outside the target, indicate no target compression and no injected field. Thus, target compression, which is observed in imploding shell-plasma compression experiments, is presumably due to the compressed H pressure.

We have used an electromagnetically imploded liner to compress an unmagnetized, dense, H plasma, and obtained radiographic evidence that this plasma was compressed to $\sim$Mbar pressure. With our existing laboratory arrangement, we are in an excellent position to evaluate critical problems with magnetized target fusion concepts. In particular, the question of contamination of a *magnetized*, hot hydrogen plasma by high-Z material from the liner (and electrodes) may be answered.

This work was supported by the Air Force Office of Scientific Research. We acknowledge the support of Dr. W. L. Baker, Dr. B. Godfrey, and Dr. R. Kelley.

*Present address: Center for Adaptive Systems Applications, Los Alamos, NM 87544.
†Also at NumerEx, Albuquerque, NM 87106.
‡Also at Maxwell Technologies Inc., Albuquerque, NM 87106.
§Also at Pennsylvania State University, University Park, PA 16802.
‖Also at Los Alamos National Laboratory, Los Alamos, NM 87545.
¶Present address: Advanced Refractory Technologies, Inc., Buffalo, NY 14207.
**Permanent address: Chemical and Nuclear Engineering, University of New Mexico, Albuquerque, NM 87131.
††Permanent address: Aerospace Engineering, University of Washington, Seattle, WA 98195.
‡‡Permanent address: Aerospace Engineering, Applied Mechanics, and Aviation, The Ohio State University, Columbus, OH 43210.

[1] I. Lindemuth and R. Kirkpatrick, Nucl. Fusion **23**, 263 (1983).
[2] I. Lindemuth *et al.*, Phys. Rev. Lett. **75**, 1953 (1995).
[3] V. K. Chernyshev and V. N. Mokhov, in *Proceedings of the 8th IEEE International Pulsed Power Conference* (IEEE, New York, 1991), pp. 395–410.
[4] C. M. Fowler, "Atomic Energy Research in the Life and Physical Sciences" (AEC Special Report, Jan. 1961), p. 104.
[5] J. G. Linhart, H. Knoepfel, and C. Gourlan, Nucl. Fusion Suppl. **2**, 733 (1962).
[6] N. K. Winsor, J. P. Boris, and R. A. Shany, in *Proceedings of the Symposium on Plasma Heating and Injection, Varenna, Italy* (Editorice Compositori, Bologna, 1973), pp. 227–231.
[7] E. P. Velikhov *et al.*, Zh. Eksp. Teor. Fiz. **43**, 429 (1973) [Sov. Phys. Tech. Phys. **18**, 274 (1973)].
[8] J. W. Shearer, University of California LLL Report No. UCID-16517, 1974.
[9] J. H. Degnan *et al.*, Phys. Rev. Lett. **74**, 98 (1995).
[10] V. Goloviznin *et al.*, in *Proceedings of the Second International Conference on Megagauss Magnetic Field Generation and Related Topics*, edited by P. J. Turchi (Plenum Press, New York, 1980), p. 415.
[11] V. K. Chernyshev *et al.*, in *Proceedings of the Sixth International Conference on Megagauss Magnetic Field Generation and Related Topics*, edited by M. Cowan and R. Spielman (Nova Science Publishers, Inc., Commack, NY, 1994), p. 815.
[12] V. Mokhov *et al.*, Sov. Phys. Dokl. **24**, 557 (1979).
[13] A. E. Sherwood *et al.*, in *Proceedings of the Second International Conference on Megagauss Magnetic Field Generation and Related Topics* (Ref. [10]), p. 391.
[14] P. J. Turchi, A. L. Cooper, R. D. Ford, D. J. Jenkins, and R. L. Burton, in *Proceedings of the Second International Conference on Megagauss Magnetic Field Generation and Related Topics* (Ref. [10]), p. 375.
[15] F. M. Lehr *et al.*, J. Appl. Phys. **75**, 3769 (1994).
[16] F. M. Lehr *et al.*, in *Proceedings of the Ninth International IEEE Pulsed Power Conference, 1993*, edited by K. R. Prestwich and W. L. Baker (IEEE, Piscataway, 1993), p. 176.
[17] J. H. Degnan *et al.*, in *Current Trends in International Fusion Research*, edited by E. Panarella (Plenum Press, New York, 1997), pp. 179–195.
[18] R. E. Peterkin, Jr., M. H. Frese, and C. R. Sovinec, J. Comp. Phys. **140**, 148 (1998).
[19] E. L. Ruden and D. E. Bell, J. Appl. Phys. **82**, 163 (1997).
[20] T. W. Hussey *et al.*, in *Proceedings of the Sixth International Conference on Megagauss Magnetic Field Generation and Related Topics* (Ref. [11]), p. 101.
[21] P-R. Chiang *et al.*, J. Appl. Phys. **76**, 637 (1994).
[22] T. W. Hussey *et al.* (to be published).